14th Australasian Fluid Mechanics Conference
Adelaide University, Adelaide, Australia
10-14 December 2001

How Accurately is a Helical Vortex Represented by Straight Segments?

D.H. Wood[1] and D. Li[2]

[2]Department of Mechanical Engineering
University of Newcastle, N.S.W., 2308 AUSTRALIA

[2]Department of Computer Science and Software Engineering
University of Newcastle, N.S.W., 2308 AUSTRALIA

Abstract

This paper assesses the accuracy of representing a helical vortex, as found in the wakes of helicopters, wind turbines, and propellers, as a sequence of straight segments. For the first time, comparison is made with recent results for the induced velocity of a helix of constant pitch and radius. Three cases are considered. The first, the velocity on the helix axis, has an analytic solution that is used to demonstrate the second order accuracy of the approximation. The second case, representing a second vortex at the same radius, shows the segments in line with the control point dominate the error. Thirdly, the self-induced velocity is determined to within an accuracy comparable with the effects of the vortex structure, of which little is presently known.

Introduction

It is common for the helical vortices in the wakes of propellers, rotors, and wind turbines to be represented computationally by a sequence of straight vortex segments, e.g. Afjeh & Keith [1], Bliss *et al.* [2], and Bhagwat & Lieshman [3, 4]. This approximation, shown schematically in Figure 1(a), has been tested thoroughly only for the known velocity field of a vortex ring, e.g. Ref.s [2 – 4]. The recently derived expressions for the self-induced motion of helical vortices by Boersma & Wood [5] and Wood & Boersma [6] allows the straight-segment approximation to be directly tested for helical vortices of constant pitch, p, and radius, R. That is the purpose of this paper.

Testing against helices rather than rings is necessary because of the small values of p in the wakes of rotors and wind turbines; in Ref. [6] it is shown that p, when normalized by R, as are all lengths in this paper, is typically about 0.05 for wind turbines and hovering rotors. This is the pitch of the helix in Figure 1(a). The figure also shows the three test cases that will be considered and Figure 2 shows the integrand for the Biot-Savart law for Case 2 for a range of p. The vortex angle θ is measured from the positive y-axis in Figure 1(a) in the direction of the helix. For small p, the nasty behaviour and the large maxima near $\theta = \pi$ in Figure 2 will obviously cause problems for any numerical method. This behaviour, which is repeated with diminishing significance every additional 2π, is caused by the proximity of the subsequent turns of the vortex and does not occur for a vortex ring. The two peaks in the integrand are displaced from π by $\theta' \approx \pm\sqrt{2\pi}\,p$. If the number of segments per revolution (during which θ increases by 2π) is $M - M = 6$ is shown in Figure 1(a) – then it is reasonable to require that $M >> \sqrt{2} / p$ for adequate representation near $\theta = \pi$.

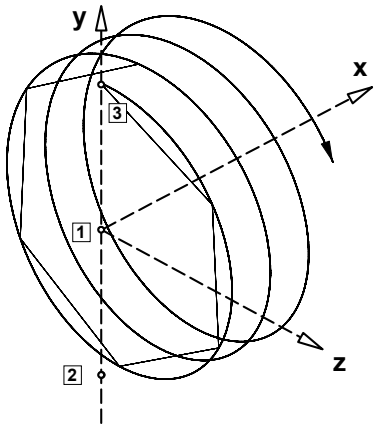

Figure 1a. Representation of helical vortex by straight segments. Only one revolution of segments is shown for $p = 0.05$ and $M = 6$.

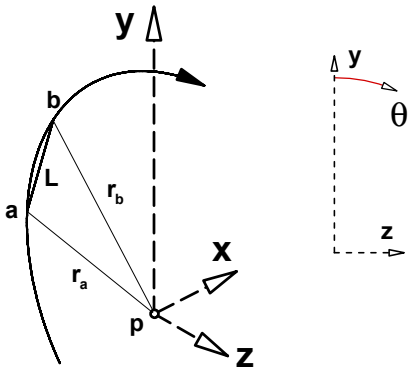

Figure 1b. Notation for Equation (4) with the control point for Case 1. The insert shows the deifnition of θ.

For $p = 0.05$, this translates to $M >> 28$. Furthermore, the integrand is zero at $\theta = \pi$ which suggests the need for M to be an even integer for Case 2.

The Test Cases

Figure 1(a) shows the three test cases for a singly-infinite helix of constant p and R beginning at $(x, y, z) = (0, 1, 0)$. In practice, this would mean that the blade shedding the helical

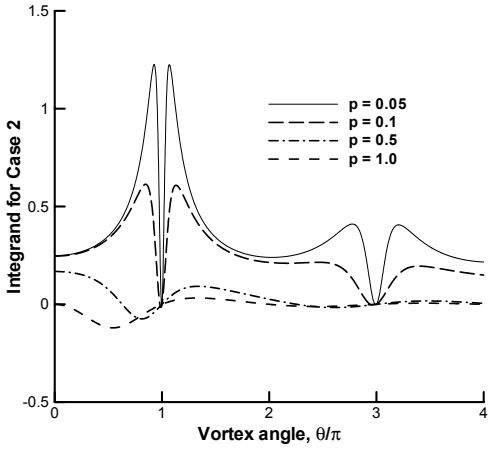

Figure 2. Integrand in Equation (1) for Case 2.

tip vortex lies along the positive y-axis ending at (0, 1, 0). In all cases, the magnitude of the induced velocities is p^{-1}, when normalised by $\Gamma/4\pi$, where Γ is the circulation. (This normalisation is used for all velocities in this paper.) The co-ordinates of the "control point" at which the velocity is to be determined for the first case are $(x_p, y_p, z_p) = (0, 0, 0)$. It is the only case with an exact solution, for the x-direction velocity, $U = p^{-1}$. This allows the determination of the order of the straight segment approximation, which is not equivalent to any simple quadrature scheme on the original Biot-Savart integral. For Case 1 the integrand decreases monotonically with θ or x.

The co-ordinates for Case 2 are $(x_p, y_p, z_p) = (0, -1, 0)$ would correspond to the tip of a second blade of a two or four-bladed rotor or turbine. It was chosen to demonstrate the essential difficulty shown in Figure 2 without the complication of the curvature singularity for the self-induced velocity in Case 3. Furthermore, Cases 2 and 3 are well suited for comparison with the results of [5, 6] who analysed doubly-infinite vortices, that is vortices which also extend infinitely in the negative x-direction. For Cases 2 and 3 we calculate the binormal velocity, U_b. For Case 2, (2.8) and (2.9) of [6] give

$$U_b = \frac{1}{\left(p^2+1\right)^{1/2}} \int_0^\infty \frac{-p^2\theta\sin\theta + \left(1-p^2\right)\left[1+\cos\theta\right]}{\left[p^2\theta^2 + 2\left\{1+\cos\theta\right\}\right]^{3/2}} d\theta \qquad (1)$$

$$= \left(p^2+1\right)^{1/2} W(\pi, p)/2 - p\left(p^2+1\right)^{-1/2}$$

where the integrand is shown in Figure 2 for a range of p and the values of $W(\pi, p)$ in Table 1 are taken from Table 1 of [6] where they are given to six significant figures. These values were obtained numerically and were checked by [6] against the asymptotic expansion of $W(\pi, p)$ for small p. For Case 3, $(x_p, y_p, z_p) = (0, 1, 0)$, which is the start of the vortex. Without the curvature term, (5.7) of Ref. [5] gives

$$U_b = \left(p^2+1\right)^{1/2} W(p)/2 - p/\left(p^2+1\right)^{1/2} + \frac{1}{2\left(p^2+1\right)}\left\{\log 2 + 2p^2 - \frac{1}{2}\log\left(p^2+1\right)\right\} \qquad (2)$$

where the values of $W(p)$ in Table 1 are also taken from Table 1 of [5] where a similar check was made against the small-p expansion. U_b is related to the x- and z-direction velocities U and W, by

$$U_b = \frac{U \pm pW}{\left(p^2+1\right)^{1/2}} \qquad (3)$$

where pW is added for Case 2 and subtracted for Case 3. For the straight-segment approximation, U and W were found as the sum of the contribution from each segment, U_s and W_s, for which the formulae are

$$\begin{bmatrix} U_s \\ W_s \end{bmatrix} = 2\frac{r_a + r_b}{r_a r_b\left[\left(r_a+r_b\right)^2 - L^2\right]} \times \begin{bmatrix} \left(y_p - y_b\right)\left(z_b - z_a\right) - \left(z_p - z_b\right)\left(y_b - y_a\right) \\ \left(x_p - x_b\right)\left(y_b - y_a\right) - \left(y_p - y_b\right)\left(x_b - x_a\right) \end{bmatrix} \qquad (4)$$

as given by Equation (2) of [1]. The subscripts "a" and "b" denote the beginning and end of each segment and the lengths r_a, r_b, and L are defined in Figure 1(b). All the calculations were to sixteen significant figures. The segments finished at a value of x determined as described in Section 4 of [5], and the remaining contribution to the infinite integral was approximated by the first method of Wood & Meyer [7].

pitch, p	***W(π, p)***	***W(p)***
0.01	99.3069	95.7022
0.05	19.3086	17.3173
0.1	9.31407	8.01822
0.5	1.53777	1.34138
1.0	0.790427	0.456367
5.0	0.190702	0.0711198

Table 1. $W(\pi, p)$ and $W(p)$

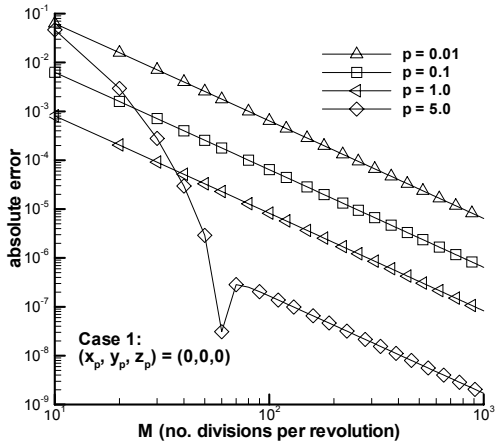

Figure 3. Absolute error for Case 1.

Results

Figure 3 shows the errors for Case 1 as a function of p and M. The error is defined as the difference between the sum of the contributions from the vortex segments plus the analytic remainder and the exact result. For convenience, the following figures show the absolute value of the error. It can be shown that the error for the first vortex segment

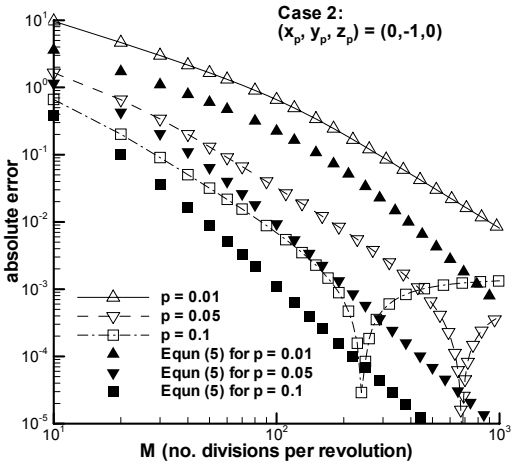

Figure 4a. Absolute error for Case 2 for small pitch.

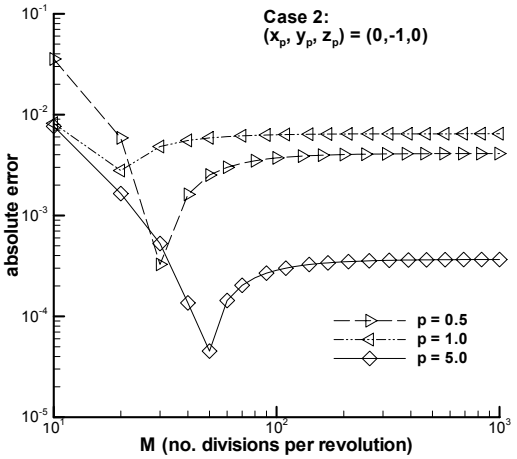

Figure 4b. Absolute error for Case 2 for large pitch.

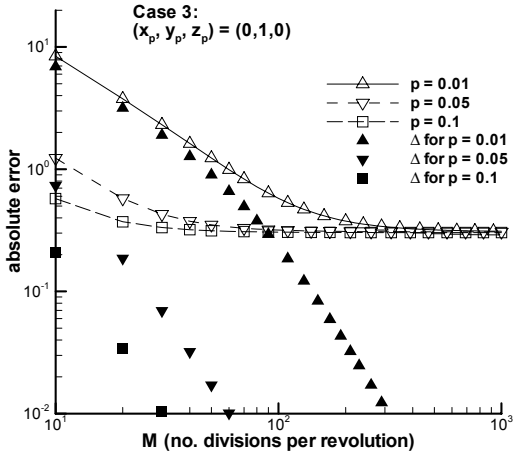

Figure 5a. Absolute error for Case 3 for small pitch

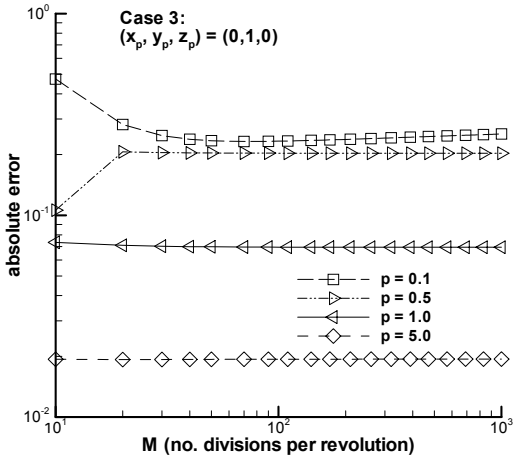

Figure 5b. Absolute error for Case 3 for large pitch.

(beginning at (0, 1, 0)) is approximately $2\pi^3M^{-3}/3$, and the calculations agree with this value. As θ increases, the error changes sign and becomes dependent on M^{-2}, which, presumably leads to the general M^{-2} dependence of the (positive) global error shown in Figure 3. This dependence was also found by [2] and [4] in their vortex ring comparisons.

The form of the error for Case 2 for small pitch, Figure 4(a), is quite different from that in Figure 3, even taking into account the limitations imposed by the six-figure accuracy of Table 1, which means, for example, that the large-M results for $p = 0.05$ and 0.1 cannot be trusted. For all values of p, the errors before (and including) the minimum absolute error are negative, and all those afterwards are positive.

At small p, the error can be estimated from the following simple analysis. All vortex segments immediately behind the control point have either y_a or $y_b = -1$, and give $U_s = 0$ by (4). (This is because the velocity induced at a point by a straight vortex segment is normal to the plane containing the point and the segment.) W_s, is more difficult to analyse, but W_s for the segment ending at $(2N+1)\pi$, where N is either zero or a positive integer, tends to cancel that for the segment immediately following. (The cancellation is exact at zero p.) Furthermore, W_s is multiplied by p in Equation (3), so that it can be ignored safely in this analysis for small p. Now the integrand in (1) is zero if $\theta = (2N+1)\pi$ for any positive integer N, so we can use the trapezoidal rule to estimate the error due to the segments beginning and ending at $(2N+1)\pi$. To the accuracy of the trapezoidal rule, this error does not depend on the $\sin\theta$ term in (1). The approximate error for each N is

$$-\frac{1}{2}\left(1+p^2\right)^{1/2}\theta'^3\left[\left\{(2N+1)\pi p\right\}^2+\theta'^2\right]^{-3/2}$$

Summing over all N, and then approximating the sum by an integral, gives the global error, Δ, as

$$\Delta \approx -\frac{\left(1+p^2\right)^{1/2}}{2pM}\left[1-\frac{p(M/2+1)}{\left\{(pM/2)^2+p^2M+p^2+1\right\}^{1/2}}+\frac{1}{2\left\{(pM/2)^2+p^2M+p^2+1\right\}^{3/2}}\right] \qquad (5)$$

The absolute value of (5) is shown in Figure 4(a) for the three lowest p. It under-estimates the error by a factor of very nearly two, but the sign and trend of the actual error with increasing M are accurately reflected by the simple formula. Furthermore, it can be shown empirically that the ratio of the actual error to Δ scales on the product pM at small pitch, at least until $pM \approx 5$. The ability of (5) to reproduce the form

of the error shows that the straight segment approximation is only first order at small M, increasing to third order at much larger values. This result could not be obtained by testing the straight segment approximation using the velocity field of a vortex ring. The analysis leading to (5) is only valid at small p, so it is not surprising that the form of the error changes markedly as p increases, Figure 4(b).

Figure 5 shows the results for Case 3, for which the Biot-Savart integrand is as given by (1) with the opposite sign for all the trigonometric terms. It behaves as θ^{-1} as $\theta \downarrow 0$, giving rise to the well-known logarithmic singularity for the self-induced velocity of any curved vortex. Expression (2) for the binormal velocity does *not* include the curvature term $-\log(\varepsilon)/2(1+p^2)$, where $\varepsilon = a/(1+p^2)$ and a is the vortex core radius, see (5.7) in Ref. [5], that arises from changing the lower limit on the Biot-Savart integral from zero to ε to avoid the singularity. This change is the basis of the "cut-off method" which is analysed in detail by Saffman [8]. Ricca [9] gives a full discussion of the singularity and its treatment for helical vortices. Furthermore, $U_s = W_s = 0$ for the first segment, as a straight vortex cannot induce any velocity on itself. An approximate correction for this error can be found by integrating the term containing θ^{-1} from $\theta = \varepsilon$ to $\theta = 2\pi/M$, the end of the first segment. For small p, the relative error in approximating the integrand by this term was found to be less than 10^{-2} for $M > 25$. Integration yields $\log(2\pi/M)/2(1+p^2)$, which was added to the binormal velocity calculated from (4). U_s from the second segment was found to be within 10% of the Biot-Savart value at small pitch, so its error was not analysed.

[5] (5.7) includes another term absent from (2): the constant, 1/4, which results from the particular assumption that the helical vortex has a circular core over which the vorticity is spread uniformly. In practice, very little is known of the structure of trailing vortices, except for those behind hovering rotors. Until this deficiency is remedied, there seems little point trying to improve upon the near-constant error of nearly 0.3 at large M in Figure 5(a). It is worth noting, however, that the value of M required to make the error constant is around 100 at small pitch. This is larger than the value used in most calculations.

The vortex segments aligned with the control point play a similar role as they did in Case 2: there is no contribution to the velocity of any segment which has either y_a or $y_b = 1$. A straightforward extension of the previous analysis (excluding the first segment!) shows Δ for Case 3 to be that given by (5) with $M/2$ in the square brackets replaced by M. Δ is shown as the solid symbols in Figure 5(a). As for case 2, this expression for Δ helps to demonstrate the first order accuracy of the straight segment approximation for small values of M. A further consequence of the usefulness of (5) and its equivalent for Case 3 is that it indicates that the determination of the velocity field of a constant diameter, constant pitch vortex is a severe test case for the straight segment approximation.

As the pitch increases, Figure 5(b), the form of the error changes significantly, for reasons similar to those advanced for Case 2.

Conclusions

This paper discusses the accuracy of representing a helical vortex by straight segments when determining the induced velocity. For the first time, the accuracy of this approximation was tested for a semi-infinite vortex of constant pitch and radius. Three test cases were considered.

The control point for Case 1 was on the centreline of the start of the vortex. Comparison with the exact solution showed the accuracy of the straight segment representation to be second order in, say, the number of vortex segments per revolution of the helix, M, and is thus the same order as the trapezoidal rule applied to the original Biot-Savart integral.

Cases 2 and 3 do not have exact solutions, so recourse was made to the recent, very accurate numerical results of Wood & Boersma [6] for the velocity of the vortex itself. The control point in the second case is displaced 180° from the vortex and the third case considered the self-induced velocity. In both these cases, attention was drawn to those vortex segments aligned with the control point as they do not contribute to the velocity. This observation, firstly, points to the necessity of using helical vortices rather than vortex rings to assess the accuracy of the straight segment approximation. Secondly, it leads to a very simple error analysis that is surprisingly useful in determining the form of the error. (5) could form the basis of a simple correction to be added to the velocities calculated using straight segments.

The error for the self-induced velocity, Case 3, tends to a constant at large M and small pitch. The magnitude of this constant is comparable to the contribution to the self-induced velocity that arises from considering the internal structure of the vortex. It would be premature to attempt to improve upon the accuracy shown in Figure 5(a) until more information is available on the internal structure of tip vortices. As the pitch increases, the error for the self-induced velocity behaves similarly to that in Case 2.

Acknowledgments

This work was funded by the Australian Research Council.

References

[1] AFJEH, A.A., and KEITH, T.G. A Simplified Free Wake Method for Horizontal-Axis Wind Turbine Performance Prediction *J. Fluids Eng'g*, **108**, 1986, 400 – 406.

[2] BLISS, D.B., TESKE, M.E., and QUACKENBUSH, T.R. A new methodology for free wake analysis using curved vortex segments. NASA CR 3958, 1987.

[3] BHAGWAT, M.J., and LEISHMAN, J.G. Stability Analysis of Helicopter Rotor Wakes in Forward Flight, *J. Amer. Helicopter Soc*., **45**, 2000, 165 – 178.

[4] BHAGWAT, M.J., and LEISHMAN, J.G. Accuracy of Straight-Line Segmentation Applied to Curvilinear Vortex Filaments. *J. Amer. Helicopter Soc*., **46**, 2001, 59 – 70.

[5] BOERSMA, J., and WOOD, D.H. On the Self-Induced Motion of a Helical Vortex, *J. Fluid Mech.,* **384**, 1999, 263 – 280.

[6] WOOD, D.H., and BOERSMA, J. On the motion of multiple helical vortices, *J. Fluid Mech.* (to appear).

[7] WOOD, D.H., and MEYER, C. Two Methods for Calculating the Velocities Induced by a Constant Diameter Far-Wake, *J. Aircraft,* **28**, 1991, 526 - 531.

[8] SAFFMAN, P.G. *Vortex Dynamics*, C.U.P.,1992.

[9] RICCA, R.L. The Effect of Torsion on the Motion of a Helical Vortex Filament, *J. Fluid Mech.,* **273**, 1994, 241 – 259.